Original papers
Nanostructured, nanoscale materials and nanodevices

УДК 537.622.6 DOI: 10.17277/jamt.2021.03.pp.167-178

The effect of Dzyaloshinskii–Moriya interaction on direct and backward transition between magnetic states of Pt/Co/Ir/Co/Pr synthetic ferrimagnet

Artem D. Talantsev[a], Ekaterina I. Kunitsyna[a], Roman B. Morgunov[a,b]✉

[a] *Institute of Problems of Chemical Physics,*
1, Academician Semenov avenue, Chernogolovka 142432, Russian Federation;
[b] *Tambov State Technical University, 106, Sovetskaya St., Tambov 392000, Russian Federation*

✉ morgunov2005@yandex.ru

Abstract: In this paper, we present the study of domain structure accompanying interstate transitions in Pt/Co/Ir/Co/Pr synthetic ferrimagnet (SF) of 1.1 nm thick and 0.6 – 1.0 nm thin ferromagnetic Co layers. Variation in the thickness of the thin layer causes noticeable changes in the domain structure and mechanism of magnetization reversal revealed by MOKE (Magneto-Optical Kerr Effect) technique. Magnetization reversal includes coherent rotation of magnetization of the ferromagnetic layers, generation of magnetic nuclei, spreading of domain walls (DW), and development of areas similar with strip domains, dependently on thickness of the thin layer. Inequivalence of the direct and backward transitions between magnetic states of SF with parallel and antiparallel magnetizations was observed in sample with thin layer thicknesses 0.8 nm and 1.0 nm. Asymmetry of the transition between these states is expressed in difference fluctuation fields and shapes of reversal magnetization nucleus contributing to the correspondent forward and backward transitions. We proposed simple model based on asymmetry of Dzyaloshinskii–Moriya interaction. This model explains competition between nucleation and domain wall propagation due to increase/decrease of the DW energy dependently on direction of the spin rotation into the DW in respect to external field.

Keywords: synthetic ferrimagnets; perpendicular anisotropy; magnetic domains; Dzyaloshinskii–Moriya interaction; MOKE.

For citation: Talantsev AD, Kunitsyna EI, Morgunov RB. Effect of Dzyaloshinskii−Moriya interaction on direct and backward transition between magnetic states of Pt/Co/Ir/Co/Pr synthetic ferrimagnet. *Journal of Advanced Materials and Technologies*. 2021;6(3):167-178. DOI: 10.17277/jamt.2021.03.pp.167-178

Влияние взаимодействия Дзялошинского–Мория на прямой и обратный переход между магнитными состояниями синтетического ферримагнетика Pt/Co/Ir/Co/Pr

А.Д. Таланцев[a], Е.И. Куницына[a], Р.Б. Моргунов[ab]✉

[a] *Институт проблем химической физики,*
пр-т Академика Семенова, 1, Черноголовка 142432, Российская Федерация;
[b] *Тамбовский государственный технический университет,*
ул. Советская, 106, Тамбов 392000, Российская Федерация

✉ morgunov2005@yandex.ru

Аннотация: Представлено исследование динамики переходов между стабильными состояниями в синтетических ферримагнетиках (СФ) Pt/Co/Ir/Co/Pr с толстыми (1,1 нм) и тонкими (0,6–1,0 нм) слоями ферромагнитного Co. Методом МОКЕ (магнитооптический эффект Керра) установлено, что изменение толщины тонкого слоя вызывает заметные изменения механизма перемагничивания. В зависимости от толщины тонкого слоя перемагничивание может происходить за счет когерентного вращения намагниченности ферромагнитных слоев, генерации зародышей намагниченности, расширения доменных стенок (ДС) и роста областей, подобных полосовым доменам. Неэквивалентность прямых и обратных переходов между магнитными состояниями синтетического ферримагнетика с параллельными и антипараллельными намагниченностями наблюдалась в образце с толщиной

тонкого слоя 0,8 и 1,0 нм. Асимметрия перехода между этими состояниями выражается в разных флуктуационных полях и формах зародышей намагниченности, вносящих вклад в соответствующие прямые и обратные переходы. Мы предложили простую модель, основанную на асимметрии взаимодействия Дзялошинского–Мория. Данная модель объясняет конкуренцию между зародышеобразованием и распространением доменной стенки за счет увеличения/уменьшения энергии ДС в зависимости от направления вращения спина в ДС по отношению к внешнему полю.

Ключевые слова: синтетические ферримагнетики; перпендикулярная анизотропия; магнитные домены; взаимодействие Дзялошинского–Мория; MOKE.

Для цитирования: Talantsev AD, Kunitsyna EI, Morgunov RB. Effect of Dzyaloshinskii–Moriya interaction on direct and backward transition between magnetic states of Pt/Co/Ir/Co/Pr synthetic ferrimagnet. *Journal of Advanced Materials and Technologies*. 2021;6(3):167-178. DOI: 10.17277/jamt.2021.03.pp.167-178

1. Introduction

Planar ferromagnetic heterostructures based on ultrathin Co layers and containing Co/Ir, Co/Pt interfaces demonstrate many unusual properties in respect of domain wall dynamics [1–19], formation of the skyrmions [20–28], and spin-orbital torque [19, 29–32]. Most of the new phenomena can be explained by contribution of the Dzyaloshinskii–Moriya interaction (DMI) in the Co/Ir and Co/Pt interfaces [1–3, 10, 13–15, 20, 24, 29, 33–41]. Synthetic ferrimagnets (SF) of Co/Ir/Co and Co/Pt/Co types are quite promising heterostructures for ultrafast magnetic memory devices [16, 26, 42]. Although magnetoresistance of the Co multilayer structures is usually small (~ 1 %), their main assignment is development of alternative technologies for information storage and processing based on spin orbit torque [42–44]. Magnetization dynamics in SF is governed by thicknesses of their layers. The variation of spacer thickness controls the sign and value of interlayer exchange coupling between ferromagnetic layers of SF [45–48]. The variation of ferromagnetic layer thickness in SF with perpendicular magnetic anisotropy (PMA) allows one to understand the role of crystalline magnetic anisotropy and its contribution to the multilayer sample properties together with interface magnetic anisotropy [12, 33, 35, 36, 40, 49]. Dependence of Co bilayer properties as a function of thickness of the Co layers, t_{Co}, demonstrates the occurrence of the perpendicular anisotropy and enhancement of DMI below $t_{Co} = 2$ nm [6, 8]. Since the analysis of net magnetic moment is often not accompanied by domain structure visualization, details of the local magnetization reversal tend to be overlooked. This can result in wrong judgment on dependence of DMI on Co layer thickness. For that reason, in this paper analysis of integral magnetic moment on t_{Co} are accompanied by detailed analysis of the magnetic nuclei.

Four stable magnetic states of SF are determined by mutual alignment of magnetizations in the layers and controlled by, both, the magnetic interlayer exchange interaction and the Zeeman energy. These energies were extracted from temperature dependences of magnetic hysteresis parameters [50, 51]. The four types of magnetic nuclei corresponding to four horizontal levels of magnetization are presented in Figure 1, in contrast with a single monolayer. Two stable "parallel" states (P^+, P^-) and two "antiparallel" (AP^+ and AP^-) states correspond to pure domainless states typical for nanosized SF. A variety of multidomain states in large ~ 1 mm^2 SF can be considered as intermediate states.

In this paper, we report on alteration of a physical origin of magnetization reversal in series of the Pt/Co/It/Co/Pt samples with progressively decreasing thicknesses of one of the Co layers. We show progressive changes in the dominating mechanism of magnetization reversal from the coherent rotation of magnetization to the multidomain magnetic structure and strip domain propagation. Competition of different channels of the magnetization reversal provides domination of one of them depending on sweeping rate of the external magnetic field ξ. We analyzed the switching field H_C for different interstate transitions in the series of the samples with different t_{Co} as a function of the magnetic field sweeping rate.

2. Materials and Methods

Multilayered structures SiO_2/Pt(3.2 nm)/Co (1.1 nm)/Ir(1.3 nm)/Co(t_{Co})/Pt(3.2 nm), t_{Co} = = 0.60 nm, 0.70 nm, 0.80 nm and 1.0 nm of 4×4 mm^2 sizes were grown by magnetron sputtering at $T = 300$ K. The methods of sample preparation and their preliminary chemical, structural and magnetic attestation were described in [50]. The thickness of 1.3 nm of the Ir spacer was selected to provide antiferromagnetic interlayer exchange coupling

comparable with the Zeeman energy. This circumstance gives an ample opportunity to switch magnetic stable states of the SF using external magnetic field.

Local *M–H* hysteresis loops and magnetic domain images were recorded by a Durham Magneto-optics NanoMOKE3 microscope based on the Kerr effect. The microscope was equipped with an electromagnet with ± 2000 Oe field range and 0.1 Oe resolution of magnetic field. MOKE measurements were performed in polar geometry (P-MOKE). The local *M–H* loops were collected from the area of a focused laser spot of 6 μm diameter. The domain images were recorded in a scanning mode from 350 × 350 μm square areas with magnification value × 270. Velocity of the domain walls (DW) was determined from a comparison of domain boundary coordinates in a series of the MOKE images recorded with 0.6 s time interval. Prior to recording, the samples were exposed in + 2000 Oe magnetic field, which exceeded the saturation field in all the samples. After that, the magnetic field was switched down to a varying negative value, and the domain images were recorded. Field stabilization time was ~ 0.1 – 0.5 s, which was less than the time interval between the frames. Time interval between frames was more, than 10 times longer than scanning time. The depth of light penetration 30–40 nm allows us to observe magnetic nuclei in top and bottom Co layers, both. We can clear distinguish four types of areas of different brightnesses corresponding to the P^+, P^-, AP^+ and AP^- states.

Brillouin light scattering (BLS) in the Damon–Eshbach geometry at room temperature was used to measure DMI coupling energy by the asymmetric frequency shift appeared from the annihilation or generation of spin waves (SWs). The laser wavelength was 532 nm; the diameter of the laser spot was 50 μm. The asymmetric frequency shift of the BLS spectrum was determined by measuring for in-plane fields $H_{IP} = +8$ kOe and $H_{IP} = -8$ kOe. As the Co films were very thin, counterpropagating surface spin waves on the top and bottom surfaces of each layer as well as spin waves in the top and bottom Co layers were simultaneously observed in the BLS experiments, averaging frequency shifts of the all layers.

3. Results and Discussion

3.1. Shape of magnetic nuclei and origin of magnetization reversal

Magnetic hysteresis loops corresponding to variation of integral Kerr rotation are presented in Figs. 1*a–d*, left panel, for the four samples with $t_{Co} = 0.6$ nm, 0.7 nm, 0.8 nm and 1.0 nm. These loops have four single domain states, P^+, P^-, AP^+ and AP^-. Depending on thin Co layer thickness and initial state of the sample, the transition between the states proceeds by different manners.

In the sample with $t_{Co} = 0.6$ nm, the $P^+ \rightarrow AP^+$ and $AP^+ \rightarrow P^+$ processes are implemented by coherent rotation of magnetization in the entire area of the film (lines *1*, *2* in Fig. 1*a*). The MOKE images for these transitions demonstrate homogeneous changes in "background" from dark to white color occurring under sweeping magnetic field. On the contrary, the $AP^- \rightarrow AP^+$ transition is provided by generation and expansion of magnetization nuclei. The $AP^- \rightarrow AP^+$ transition is accompanied by replacing black to white areas with no intermediate colors (line *3* in Fig. 1*a*). There are two magnetization phases AP^- and AP^+ separated by 180° domain walls.

The rest of the samples with $t_{Co} = 0.7$ nm – 1.0 nm show the formation of nuclei of several types. In the $t_{Co} = 0.7$ nm sample, the P^+ and AP^+ domains formed in the $P^+ \rightarrow AP^+$ and $AP^+ \rightarrow P^+$ transitions are of similar shapes (lines *1*, *2* in Fig. 1*b*). However, the shape of the AP^+ areas formed in the $AP^- \rightarrow AP^+$ transition (line *3* in Fig. 1*b*) differs from the shape of the AP^+ areas formed in the $P^+ \rightarrow AP^+$ transition (lines 1, *2* in Fig. 1*b*). Thus, the shape of the nuclei is not sensitive to mutual orientation of magnetization in a final state of transition (P^+ or AP^+), but the shape depends on the layer (top or bottom), where transition occurs. This fact is expectable because the individual maps of nucleation centers (defects) distribution are different in top and bottom layers. Reproducible decoration of the horizontal scratch in lines *1*, *2* in Fig. 1*b* indicates the nuclei in the same top layer, while the absence of scratches in line *3* in Fig. 1*b* indicates nuclei of the bottom layer.

On the contrary, in the samples with $t_{Co} = 0.8$ and 1.0 nm, the $P^+ \rightarrow AP^+$ and $AP^+ \rightarrow P^+$ transitions accompanied with domains of different shapes (compare lines *1*, *2* in Figs. 1*c*, *d*). The $AP^+ \rightarrow P^+$ transition is provided by nucleation of many small round areas of reversed magnetization, decorating scratches, while backward process $P^+ \rightarrow AP^+$ is accompanied by stripe domains as well as for $AP^- \rightarrow AP^+$ transition.

Thus, the shape of domains in "thick" samples becomes independent of the reversing layer, but the shape is sensitive to mutual orientation of magnetizations at the final state of transition.

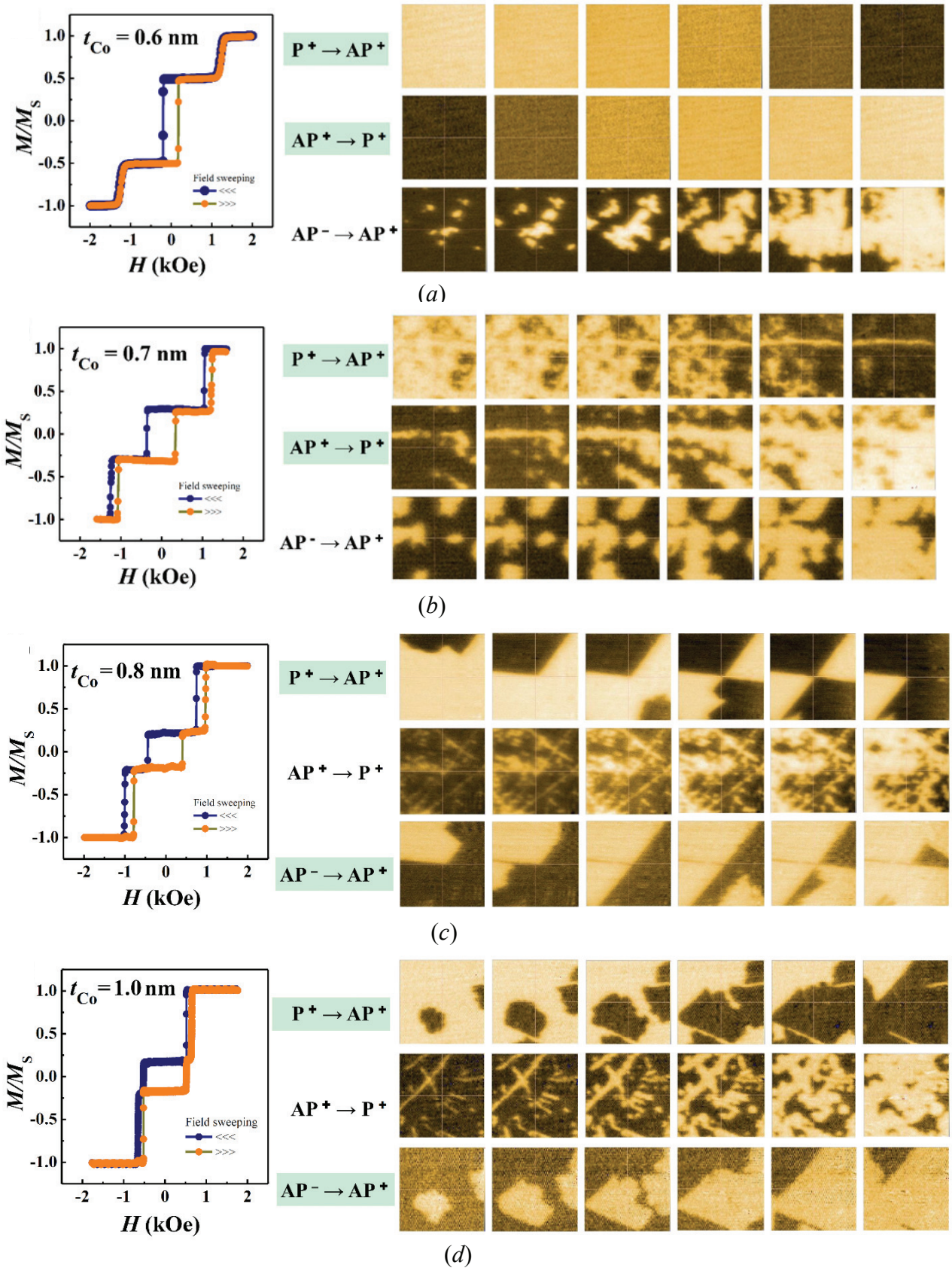

Fig. 1. Left panel: *M–H* loops for the t_{Co} = 0.6 – 1.0 nm samples recorded at 0.1 kOe/s magnetic field sweeping rate. Right panel: MOKE images captured for Pt/Co(*x*)/Ir/Co(1.0 nm)/Pt heterostructure (*x* = 0.6, 0.7, 0.8 and 1.0 nm), for $P^+ \rightarrow AP^+$, $AP^+ \rightarrow P^+$ and $AP^+ \rightarrow AP^-$ transitions

Variation of the top Co layer thickness in the 0.6 – 1.0 nm range enables to tune the magnetic nuclei shapes. There are two intervals of Co layer thickness: (1) presence of the thin layer the domain shape depends on the layer, which magnetization is changed in external field (independently on direction of the transition), (2) in the case of thicker top layer, mutual orientation of magnetizations of the layers in their final states (parallel or antiparallel) fully predetermines nuclei shapes (independently on that, which layer magnetization is reversed).

3.2. Thermal activation of the magnetic nuclei

The regularities of nuclei formation depend on thermodynamic parameters of nucleation such as fluctuation field H_f, activation volume V_A, and activation energy E_A. In this section, we will determine these parameters and analyze their sensitivity to magnetic field sweeping rate.

The dependences of switching fields H_C on magnetic field sweeping rate are not linear for all Co thicknesses and all transitions (Fig. 2), except two rate independent transitions in the sample t_{Co} = = 0.6 nm (Fig. 2*a*, *b*).

Fluctuation field H_f was determined from the slope of the dependence of switching field H_C on sweeping rate dH/dt plotted in a semi-logarithmic scale. Linear approximations of these dependences at low (below 0.01 kOe/s) and high (over 1 kOe/s) sweeping rates determine the range of fluctuation fields for each transition. Fluctuation field H_f ranges are represented for different samples in Fig. 3. The mean values of fluctuation fields for different transitions in all samples are summarized in Fig. 4.

The width of an accessible fluctuation field range and the middle of fluctuation field range grow with increasing t_{Co}, and suddenly decrease at t_{Co} = 1.0 nm for the $AP^- \rightarrow AP^+$ and $AP^+ \rightarrow P^+$ transitions, both. The fluctuation field of the $P^+ \rightarrow AP^+$ transition varies non-monotonically with t_{Co}. It is surprising, that the H_f ranges for the $AP^+ \rightarrow P^+$ and $P^+ \rightarrow AP^+$ transitions do not coincide.

The activation volume was estimated from fluctuation field using the fact of proportionality of the layers saturation magnetizations M_{S1} and M_{S2} to correspondent thicknesses t_1 and t_2:

$$V_A = kT(t_2 + t_1)/2H_f M_S h_1 \qquad (1)$$

for the $P^+ \rightarrow AP^+$ and $AP^+ \rightarrow P^+$ transitions, and

$$V_A = kT(t_2 + t_1)/2H_f M_S(t_2 - t_1) \qquad (2)$$

for the $AP^- \rightarrow AP^+$ transition. The difference between expressions (1) and (2) is that the $P^+ \rightarrow AP^+$ process occurs by upper layer magnetization reversal, while the $AP^- \rightarrow AP^+$ process proceeds by magnetization reversal of both layers possessing integral magnetization proportional to $M_{S2} - M_{S1} \approx t_2 - t_1$.

The activation volume of the $AP^- \rightarrow AP^+$ transition (green bars in Fig. 4*b*) is almost the same for 0.6, 0.7 and 0.8 nm samples. Therefore, the thickness of free layer does not affect the mechanism of the $AP^- \rightarrow AP^+$ transition.

The high value of activation volume for 1.0 nm sample can be caused by the difference between the actual value of Co layer thickness and that determined from the deposition rate. As the difference between t_1 and t_2 is in the denominator of Eq. (2), and in the 1.0 nm sample the thicknesses of the thin and thick layers are of almost same values (1.0 and 1.1 nm), the error of 10 % in both thicknesses will result in variations of V_A up to 6 times.

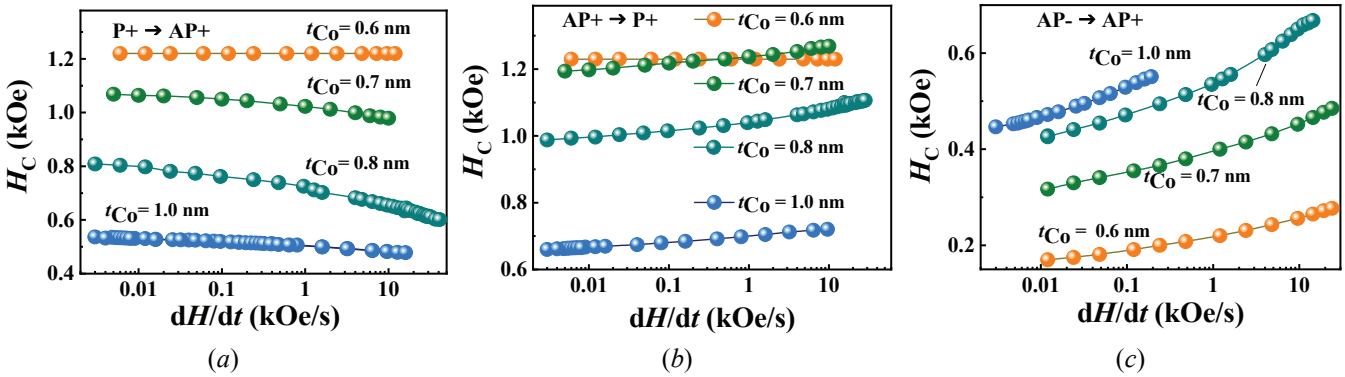

Fig. 2. Dependences of switching fields on magnetic field sweeping rate for $P^+ \rightarrow AP^+$ (*a*), $AP^+ \rightarrow P^+$ (*b*) and $AP^- \rightarrow AP^+$ (*c*) transitions

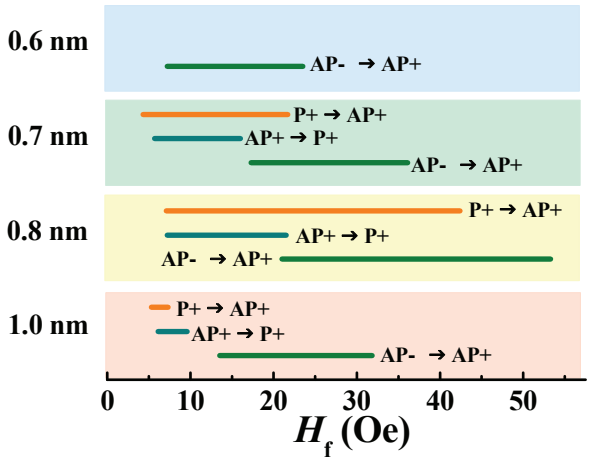

Fig. 3. Ranges of fluctuation fields for samples with $t_{Co} = 0.6$, 0.7, 0.8 and 1.0 nm for the $P^+ \rightarrow AP^+$, $AP^+ \rightarrow P^+$ and $AP^- \rightarrow AP^+$ transitions. Lines corresponding to the same types of transitions are shown by the same color

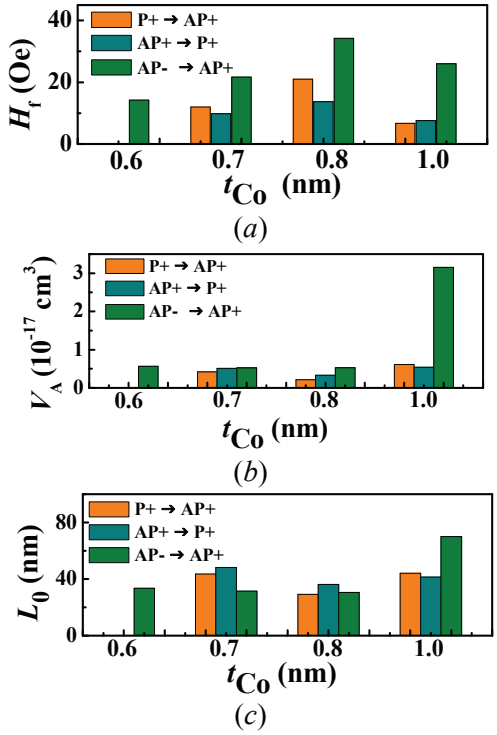

Fig. 4. Dependences of fluctuation field (*a*), activation volume (*b*) and lateral size of domain nuclei (*c*) on thickness t_{Co} of Co thin layer for the $P^+ \rightarrow AP^+$, $AP^+ \rightarrow P^+$ and $AP^- \rightarrow AP^+$ transitions

In contrast to the $AP^- \rightarrow AP^+$ transition, the activation volume for the $P^+ \rightarrow AP^+$ and $AP^+ \rightarrow P^+$ transitions (orange and blue bars in Fig. 4*b*) are sensitive to the thickness of Co free layer. From the comparison of 0.7 and 0.8 nm samples (for 0.6 sample the fluctuation field of these transitions is zero and the activation volume is not determined), one can conclude that the increase in thickness of Co free layer results in reduction of activation volumes of the $P^+ \rightarrow AP^+$ and $AP^+ \rightarrow P^+$ transitions.

From the determined values of activation volume, the lateral size of domain nuclei can be estimated. As layer thicknesses are $t_{Co} \sim t_1 \sim 1$ nm $= 10^{-7}$ cm and activation volumes are of an order of 10^{-17} cm^3, the domain nucleation area is of an order of 10^{-10} cm^2, and lateral size of nuclei is $L_0 \sim 10^{-5}$ cm $= 100$ nm. Lateral size of nuclei of different types can be calculated accurately by formula $L_0 = \sqrt{V_A / \pi t_1}$ for the $P^+ \rightarrow AP^+$ and $AP^+ \rightarrow P^+$ transitions, and by formula $L_0 = \sqrt{V_A / \pi (t_1 + t_2)}$ for the $AP^- \rightarrow AP^+$ transition. The size of nuclei for the $P^+ \rightarrow AP^+$, $AP^+ \rightarrow P^+$ and $AP^- \rightarrow AP^+$ transitions are given in Fig. 4*c*.

The lateral nuclei size is always out of resolution of Kerr microscope, being ~10 times lower than light wavelength. Thus, we can not judge about initial stages of nucleation. For that reason, very fast generation of small non resolvable nuclei in the sample with $t_{Co} = 0.6$ nm can give images similar to images in lines *1* and *2* in Fig. 1. Zero value of fluctuation field in this sample disproves this assumption because thermally activated nuclei generation should possess finite activation parameters and volume compatible with values in Fig. 4*c*. Thus, we cannot explain the absence of magnetization nuclei in images in lines *1* and *2* of Fig. 1 by low resolution of Kerr microscope. Reasonable origin of the magnetization reversal in the $P^+ \rightarrow AP^+$, $AP^+ \rightarrow P^+$ transitions is coherent rotation of magnetization under external magnetic field.

The unresolvable size of the nuclei obviously plays a role in explanation of the stripe like areas limited by scratches (lines *1* and 3, Fig. 1*c*, *d*). The stripe domains have not been observed yet in structures with perpendicular anisotropy due to their energetically unfavourable structure and size. For that reasons seeming of the strip domain in our experiments is probably an artefact caused by low resolution of Kerr microscope. Most probably the space limited by scratches was rapidly filled out by small non resolvable nuclei seeming like continuous area of the same continuous direction of magnetization. Thus, one should distinguish magnetization areas filled by nuclei of the magnetic phase and expanded magnetic nuclei also observable when velocity of the domain walls is high enough to enlarge nuclei size until their visible length of ~ 1 μm.

3.3. Contribution of Dzyaloshinskii-Moriya interaction to magnetization reversal

The Dzyaloshinskii-Moriya antisymmetric exchange interaction leads to noncollinear and chiral ordering of spins. The DMI plays an important role in spin orbitronics [2, 3]. The interfacial DMI arises in thin ferromagnetic films at the interface with heavy metals, where the spin-orbit interaction (SOC) of two adjacent spins of the ferromagnetic film S_i and S_j propagates through the exchange interaction with a heavy metal atom located in an adjacent non-magnetic layer. This type of DMI implying the absence of the inversion symmetry in interface region is described in the framework of the three-site Lévy–Fert model [1].

The interfacial DMI was experimentally studied in wide series of Co based samples, where Co/Ir and Co/Pr interfaces are presented. Asymmetry of bubble expansion in the in-plane magnetic field allowed to estimate equivalent DMI field in Pt/Co/Pt, Pt/Co/Ir/Pt [7], Pt/Co/Ir [12], Pt/Co/Pt [8], Pt/Co/Ir [18], Pt/Co/Pt [19] lying in the 0.5 – 2.5 erg/cm^3 range dependently on interface quality, Co thickness, type of the heavy metal and spacer properties.

In the case, when both the top and bottom ferromagnetic layers of the SFs are coupled with the interlayer by DMI, different directions of the domain wall magnetization should be considered. Since symmetry of the DMI and Heisenberg exchange energy J are different, the change of the spin rotation direction in the Neel wall (Fig. 1) causes change of the sign of DMI energy density D, and does not affect J value. The $P^+ \rightarrow AP^+$ and $AP^+ \rightarrow P^+$ transitions, both, have same spin rotation direction in the domain wall of upper Co layer. Another reason to change the sign of DMI is to change the direction of the domain wall propagation. In this case both J and D change their sign. The difference in the sign of DMI in the upper Co layer, when $P^+ \rightarrow AP^+$ transition is changed to $AP^+ \rightarrow P^+$ transition leads to difference between energy of the domain wall and to corresponding change in the domain wall velocity.

One of the most reliable techniques to measure coupling energy D is Brillouin light scattering (BLS) used in our experiments.

A typical BLS spectrum recorded in direct (red line) and opposite (blue line) directions of in-plane applied 8 kOe magnetic fields at T = 300 K and wave vector k_x = 11 μm^{-1} is shown in Fig. 5.

The Damon–Eshbach geometry was used to determine D value, i.e. magnetization of sample lied in sample plane perpendicularly to the wave vector k_x. We applied in plane field H_{IP} equal to magnetic anisotropy field H_A = 10 kOe determined by SQUID magnetometer to satisfy the above mentioned conditions. One can see presence of the two peaks with maximums in positive and negative magnetic fields. These two peaks correspond to the Stokes and anti-Stokes BLS components. Change of magnetic field H_{IP} to opposite direction causes shift of the Stokes and anti-Stokes maximums, replacing their frequency positions f, but frequency difference Δf between them remains constant (Fig. 5). The origin of the alteration of the Stokes and anti-Stokes maximums is interfacing DMI, which coupling energy D is directly proportional to Δf value:

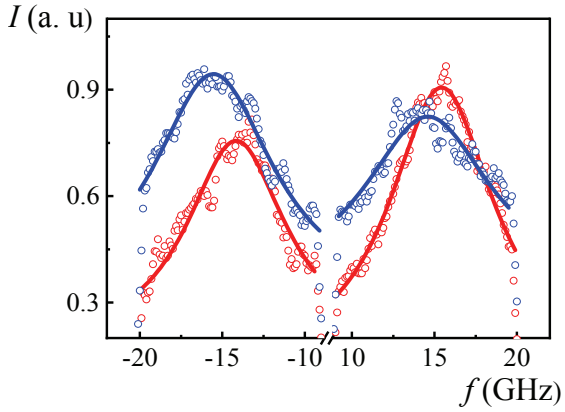

Fig. 5. Normalized BLS spectra recorded in direct (red line) and opposite (blue line) directions of applied magnetic fields 8 kOe at T = 300 K and wave vector k_x = 11 μm^{-1}

$$D = \frac{\Delta f \pi M_S}{2\gamma k_x}, \qquad (3)$$

γ is gyromagnetic ratio, k_x is the x component of the wave vector, depending on incidence angle, M_S is saturation magnetization. Extraction of frequencies of the Stokes and anti-Stokes lines from Fig. 5 and calculation of DMI by formula (3) results in D = 1.1 erg/cm^2, quite similar with the value obtained by other authors in similar samples.

In the presence of DMI in the sample, an effective field consists of the external constant field H_{IP} and H_{DMI} directed, both, in plane of the sample. The effective in-plane field of the sample affects the velocity of the domain walls. This circumstance can be used to estimate the strength and sign of DMI contributing to domain wall velocity [7, 8]. We use the equation for the motion of the domain wall in creep mode to find the relationship between the speed

of the domain wall v and the H_{DMI} field in creep mode:

$$v = v_0 \exp\left(-\zeta(H)^{-\mu}\right), \quad (4)$$

v_0 is constant velocity, H is out-of-plane magnetic field, ζ is scaling coefficient, exponent $\mu = 1/4$ is parameter corresponding to creep regime.

According to [8], ζ parameter depends on energy density of the domain wall and in-plane field H_{IP}:

$$\zeta = \zeta_0 [\sigma_{DW}(H_{DMI})/\sigma_0]^{1/4}, \quad (5)$$

where ζ_0 is scaling coefficient, σ_{DW} is energy density of the domain wall, σ_0 is energy density of the Bloch-type domain wall.

According to [8], dependence of the density of domain wall energy σ_{DW} on DMI field H_{DMI} can be expressed as:

$$\sigma_{DW} = \sigma_0 \pm \frac{\Delta\pi^2 M_S^2 H_{DMI}^2}{8K_D}. \quad (6)$$

Expression (6) can be applied with a limitation $|H_{IP} + H_{DMI}| < 4K_D/\pi M_S$. In the studied sample with anisotropy field ~ 8 kOe, this limitation is fulfilled in zero in-plane fields. The sign "+" or "–" in expression (8) is determined by direction of DMI field in respect to the magnetic nuclei border. Energy density of the AP^+/P^+ border is obviously controlled by DMI, which sign (positive or negative) depends on mutual orientations of the top and bottom Co layers. Substitution of (6) to (5) and to (4) results in expression:

$$\ln(v/v_0) = \zeta_0 \left(1 \pm \frac{\Delta\pi^2 M_S^2 H_{DMI}^2}{8\sigma_0 K_D}\right)^{1/4} H^{-1/4}. \quad (7)$$

Approximations of field dependences by formula (7) are shown in Figs. 6 and 7 for different transitions and different thicknesses of the upper layer.

One can find a different sign of the slope in $v_{DW}(H)$ coordinates (Fig. 6*a*) and very close slopes for the samples of different upper layer thicknesses (Fig. 6*b*). Figure 6*b* allows one to conclude very high accuracy of comparison of the slopes even in different samples.

If we modify Fig. 6*a*, plotting modulus of the DW velocity (Fig. 7), we can compare slopes of the $v_{DW}(H)$ dependences for opposite processes $P^+ \rightarrow AP^+$ and $AP^+ \rightarrow P^+$. There is an obvious difference in the slopes of the $v_{DW}(H)$ dependences. This difference indicates different activation energies

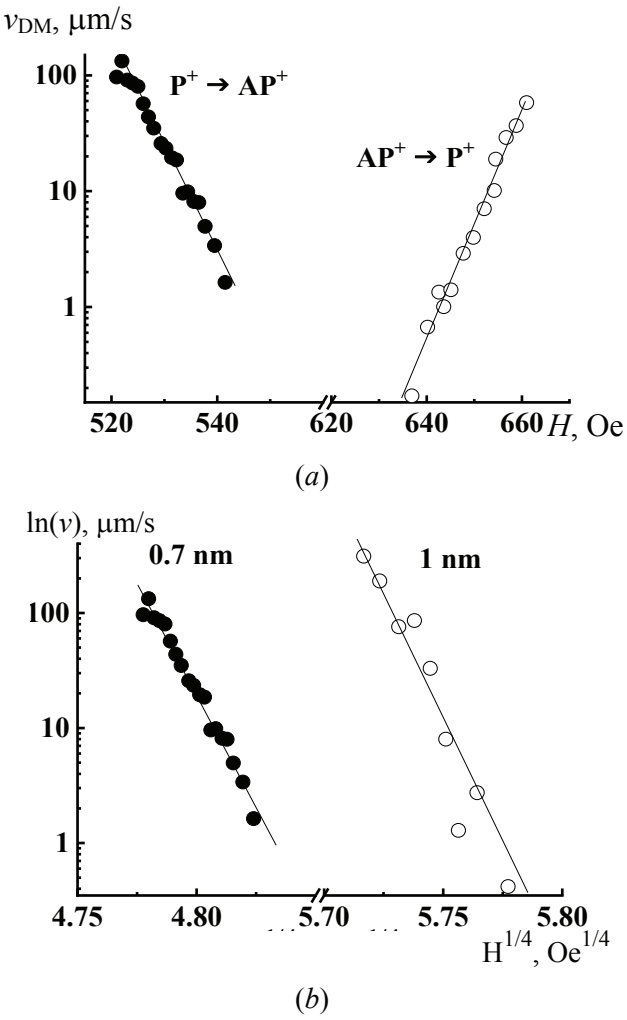

Fig. 6. Field dependences of the velocity of motion of the domain wall AP^+ during the transition $P^+ \rightarrow AP^+$ and $AP^+ \rightarrow P^+$ (*a*); comparison of the field dependences for $P^+ \rightarrow AP^+$ transition in samples of different thicknesses of upper layer (*b*). Solid lines are approximations by formula (7)

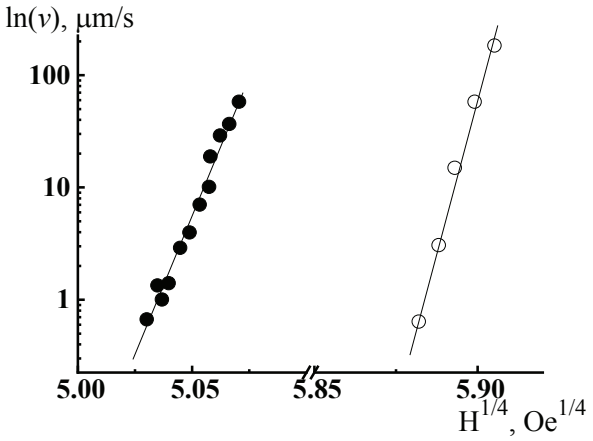

Fig. 7. Field dependences of the modulus of the velocity of motion of the domain wall P^+ during the transition $AP^+ \rightarrow P^+$

for direct and backward transitions. According to formula (7) this difference can be explained by contribution of the DMI field, increasing and decreasing potential barriers in direct and backward processes, respectively.

4. Conclusions

1. The physical process driving magnetization reversal of the thin layer without changes in magnetization of the thick 1.1 nm layer (the $P^+ \rightarrow AP^+$, $AP^+ \rightarrow P^+$ transitions) is controlled by thin layer thickness.

For $t_{Co} \leq 0.6$ nm magnetization reversal is caused by coherent rotation of magnetization of the layer on the whole in the field interval of 1–20 Oe. The fluctuation field of this process was determined as zero indicating the absence of the magnetization nuclei.

For $t_{Co} = 0.7$ nm the forward and reverse $P^+ \rightarrow AP^+$, $AP^+ \rightarrow P^+$ transitions are equivalent and they proceed by generation of nuclei.

For $t_{Co} = 0.8$–1.0 nm the forward $P^+ \rightarrow AP^+$ and backward $AP^+ \rightarrow P^+$ processes become inequivalent. Forward transition is provided by small number of nuclei rapidly expanding by domain wall motion. Backward transition $AP^+ \rightarrow P^+$ is provided by generation of great number of nuclei with small contribution of their expansion.

2. Activation volume of the $P^+ \rightarrow AP^+$ and $AP^+ \rightarrow P^+$ transitions depends on the ratio of thicknesses of thin and thick layers. Similarity of shape of the magnetization areas filled by nuclei of the final state for the $P^+ \rightarrow AP^+$ and $AP^+ \rightarrow P^+$ transitions correlates with ratio of activation volumes of these transitions. When the activation volumes of the $P^+ \rightarrow AP^+$ and $AP^+ \rightarrow P^+$ transitions are close to each other ($t_{Co} = 0.7$ nm), magnetization reversal areas shapes are determined by those layer, which magnetization reverses. At higher thickness ($t_{Co} = 0.8 - 1.0$ nm) activation volumes of the $P^+ \rightarrow AP^+$ and $AP^+ \rightarrow P^+$ transitions become different, and the shape of magnetization area is determined by final state of transition independently on that, which layer is involved in magnetization reversal.

3. Change of the DMI sign in forward $P^+ \rightarrow AP^+$ and backward $AP^+ \rightarrow P^+$ domain wall motion makes different energy densities of the domain wall in these DW motion modes. The correspondent increase in the DW velocity in forward $P^+ \rightarrow AP^+$ transition provides domination of the magnetization reversal by magnetic nuclei expansion. Decrease in the DW velocity in backward $AP^+ \rightarrow P^+$ transition provides domination of nucleation type of the magnetization reversal.

5. Funding

This study was supported by Grant of President of Russian Federation for Scientific School 2644.2020.2 and the State Assignment of the Institute of Problems of Chemical Physics, Russian Academy of Sciences (Project No. AAAA-A19-119092390079-8).

6. Acknowledgements

We are grateful to Prof. A. Fert, Prof. S. Mangin and Prof. A.K. Zvezdin for fruitful discussions.

7. Conflict of interests

The authors declare no conflict of interest.

References

1. Cao A, Zhang X, Koopmans B, Peng S, Zhang Y, Wang Z, et al. Tuning the Dzyaloshinskii–Moriya interaction in Pt/Co/MgO heterostructures through the MgO thickness. *Nanoscale*. 2018;10(25):12062-12067. DOI:10.1039/c7nr08085a

2. Kwon J, Hwang H-K, Hong J-Il, You C-Y. Bidirectional propagation of tilting domain walls in perpendicularly magnetized T shaped structure with the interfacial Dzyaloshinskii-Moriya interaction. *Scientific Reports*. 2018;8(1):18035(1-8). DOI:10.1038/s41598-018-36523-9

3. Yoshimura Y, Kim KJ, Taniguchi T, Tono T, Ueda K, Hiramatsu R, et al. Soliton-like magnetic domain wall motion induced by the interfacial Dzyaloshinskii–Moriya interaction. *Nature Physics*. 2016;12(2):157-161. DOI:10.1038/NPHYS3535

4. Fache T, Tarazona HS, Liu J, L'vova G, Applegate MJ, Rojas-Sanchez JC, et al. Nonmonotonic aftereffect measurements in perpendicular synthetic ferrimagnets. *Physical Review B*. 2018;98(6):064410(1-8). DOI:10.1103/PhysRevB.98.064410

5. Morgunov RB, Kunitsyna EI, Talantsev AD, Koplak O V, Fache T, Lu Y, Mangin S. Influence of the magnetic field sweeping rate on magnetic transitions in synthetic ferrimagnets with perpendicular anisotropy. *Applied Physics Letters*. 2019;114(22):222402(1-6). DOI:10.1063/1.5096951

6. Talantsev A, Lu Y, Fache T, Lavanant M, Hamadeh A, Aristov A, Koplak O, et al. Relaxation dynamics of magnetization transitions in synthetic antiferromagnet with perpendicular anisotropy. *Journal of*

Physics: Condensed Matter. 2018;30(13):135804. DOI:10.1088/1361-648X/aaaf04

7. Kirilyuk A, Ferré J, Grolier V, Jamet JP, Renard D. Magnetization reversal in ultrathin ferromagnetic films with perpendicular anisotropy. *Journal of Magnetism and Magnetic Materials*. 1997;171(1-2):45-63. DOI:10.1016/S0304-8853(96)00744-5

8. Morgunov RB, L'vova GL, Talantsev AD, Koplak OV, Fache T, Mangin S. Effect of Co layer thickness on magnetic relaxation in Pt/Co/Ir/Co/Pt/GaAs spin valve. *Journal of Magnetism and Magnetic Materials*. 2018;459:33-36. DOI:10.1016/j.jmmm.2017.12.083

9. Morgunov RB, L'vova GL. Slow oscillations of the perpendicular magnetization of the Pt/Co/Ir/Co/Pt spin valve. *JETP Letters*. 2018;108(2):137-141. DOI:10.1134/S0021364018140102

10. Perini M, Meyer S, Dupé B, Von Malottki S, Kubetzka A, Von Bergmann K, et al. Domain walls and Dzyaloshinskii-Moriya interaction in epitaxial Co/Ir(111) and Pt/Co/Ir(111). *Physical Review B*. 2018;97(18):184425(1-8). DOI:10.1103/PhysRevB.97.184425

11 Lemerle S, Ferré J, Chappert C, Mathet V, Giamarchi T, Le Doussal P. Domain wall creep in an ising ultrathin magnetic film. *Physical Review Letters*. 1998;80(4):849-852. DOI:10.1103/PhysRevLett.80.849

12. Metaxas PJ, Jamet JP, Mougin A, Cormier M, Ferré J, Baltz V, et al. Creep and flow regimes of magnetic domain-wall motion in ultrathin Pt/Co/Pt films with perpendicular anisotropy. *Physical Review Letters*. 2007;99(21):217208(1-4). DOI:10.1103/PhysRevLett.99.217208

13. Kwon J, Goolaup S, Gan WL, Chang CH, Roy K, Lew WS. Asymmetrical domain wall propagation in bifurcated PMA wire structure due to the Dzyaloshinskii-Moriya interaction. *Physical Review Letters*. 2017;110(23):232402. DOI:10.1063/1.4984750

14. Hrabec A, Porter NA, Wells A, Benitez MJ, Burnell G, McVitie S, et al. Measuring and tailoring the Dzyaloshinskii-Moriya interaction in perpendicularly magnetized thin films. *Physical Review B*. 2014;90(2):020402(1-5). DOI:10.1103/PhysRevB.90.020402

15. Ajejas F, Křižáková V, De Souza Chaves D, Vogel J, Perna P, Guerrero R, et al. Tuning domain wall velocity with Dzyaloshinskii-Moriya interaction. *Physical Review Letters*. 2017;111(20):202402. DOI:10.1063/1.5005798

16. Yang SH, Ryu KS, Parkin S. Domain-wall velocities of up to 750 m s^{-1} driven by exchange-coupling torque in synthetic antiferromagnets. *Nature Nanotechnology*. 2015;10(3):221-226. DOI: 10.1038/nnano.2014.324

17. Miron IM, Moore T, Szambolics H, Buda-Prejbeanu LD, Auffret S, Rodmacq B, et al. Fast current-induced domain-wall motion controlled by the Rashba effect. *Nature Materials*. 2011;10(6):419-423. DOI:10.1038/nmat3020

18. Emori S, Bauer U, Ahn SM, Martinez E, Beach GSD. Current-driven dynamics of chiral ferromagnetic domain walls. *Nature Materials*. 2013;12(7):611(1-6). DOI:10.1038/nmat3675

19. Ryu KS, Thomas L, Yang SH, Parkin S. Chiral spin torque at magnetic domain walls. *Nature Nanotechnology*. 2013;8(7):527-533. DOI:10.1038/nnano.2013.102D

20. Moreau-Luchaire C, Moutafis C, Reyren N, Sampaio J, Vaz CAF, Van Horne N, et al. Additive interfacial chiral interaction in multilayers for stabilization of small individual skyrmions at room temperature. *Nature Nanotechnology*. 2016;11(5):444-448. DOI:10.1038/NNANO.2015.313

21. Soumyanarayanan A, Raju M, Oyarce ALG, Tan AKC, Im MY, Petrovic AP, et al. Tunable room-temperature magnetic skyrmions in Ir/Fe/Co/Pt multilayers. *Nature Materials*. 2017;16(9):898-904. DOI:10.1038/NMAT4934

22. Boulle O, Vogel J, Yang H, Pizzini S, De Souza Chaves D, Locatelli A, et al. Room-temperature chiral magnetic skyrmions in ultrathin magnetic nanostructures. *Nature Nanotechnology*. 2016;11(5):449-454. DOI:10.1038/NNANO.2015.315

23. Miao BF, Sun L, Wu YW, Tao XD, Xiong X, Wen Y, et al. Experimental realization of two-dimensional artificial skyrmion crystals at room temperature. *Physical Review B*. 2014;90(17):174411(1-5). DOI:10.1103/PhysRevB.90.174411

24. Fert A, Reyren N, Cros V. Magnetic skyrmions: Advances in physics and potential applications. *Nature Reviews Materials*. 2017;2:17031. DOI:10.1038/natrevmats.2017.31

25. Rohart S, Miltat J, Thiaville A. Path to collapse for an isolated Néel skyrmion. *Physical Review B*. 2016;93(21):214412(1-6). DOI:10.1103/PhysRevB.93.214412

26. Stosic D, Ludermir TB, Milošević MV. Pinning of magnetic skyrmions in a monolayer Co film on Pt(111): Theoretical characterization and exemplified utilization. *Physical Review B*. 2017;96(21):214403(1-11) DOI: 10.1103/PhysRevB.96.214403

27. Hrabec A, Sampaio J, Belmeguenai M, Gross I, Weil R, Chérif SM, et al. Current-induced skyrmion generation and dynamics in symmetric bilayers. *Nature Communications*. 2017;8:15765(1-6). DOI:10.1038/ncomms15765

28. Pollard SD, Garlow JA, Yu J, Wang Z, Zhu Y, Yang H. Observation of stable Néel skyrmions in cobalt/palladium multilayers with Lorentz transmission electron microscopy. *Nature Communications*. 2017;8:14761(1-8). DOI:10.1038/ncomms14761

29. Khadka D, Karayev S, Huang SX. Dzyaloshinskii–Moriya interaction in Pt/Co/Ir and Pt/Co/Ru multilayer films. *Journal of Applied Physics*. 2018;123(12):123905. DOI:10.1063/1.5021090

30. Pai CF, Mann M, Tan AJ, Beach GSD. Determination of spin torque efficiencies in heterostructures with perpendicular magnetic anisotropy. *Physical Review B*. 2016;93(14):144409(1-7). DOI:10.1103/PhysRevB.93.144409

31. Miron IM, Gaudin G, Auffret S, Rodmacq B, Schuhl A, Pizzini S, et al. Current-driven spin torque induced by the Rashba effect in a ferromagnetic metal layer. *Nature Materials*. 2010;9(3):230-234. DOI:10.1038/nmat2613

32. Kim KW, Seo SM, Ryu J, Lee KJ, Lee HW. Magnetization dynamics induced by in-plane currents in ultrathin magnetic nanostructures with Rashba spin-orbit coupling. *Physical Review B*. 2012;85(18):180404(1-5). DOI:10.1103/PhysRevB.85.180404

33. Rowan-Robinson RM, Stashkevich AA, Roussigné Y, Belmeguenai M, Chérif SM, Thiaville A, et al. The interfacial nature of proximity-induced magnetism and the Dzyaloshinskii-Moriya interaction at the Pt/Co interface. *Scientific Reports*. 2017;7(1):16835(1-11). DOI:10.1038/s41598-017-17137-z

34. Ziemys G, Ahrens V, Mendisch S, Csaba G, Becherer M. Speeding up nanomagnetic logic by DMI enhanced Pt/Co/Ir films. *AIP Advances*. 2018;8(5):056310. DOI:10.1063/1.5007308

35. Kim NH, Jung J, Cho J, Han DS, Yin Y, Kim JS, et al. Interfacial Dzyaloshinskii-Moriya interaction, surface anisotropy energy, and spin pumping at spin orbit coupled Ir/Co interface. *Physical Review Letters*. 2016;108(14):142406. DOI:10.1063/1.4945685

36. Ishikuro Y, Kawaguchi M, Kato N, Lau YC, Hayashi M. Dzyaloshinskii-Moriya interaction and spin-orbit torque at the Ir/Co interface. *Physical Review B*. 2019;99(13):134421(1-6). DOI:10.1103/PhysRevB.99.134421

37. Jaiswal S, Litzius K, Lemesh I, Büttner F, Finizio S, Raabe J, et al. Investigation of the Dzyaloshinskii-Moriya interaction and room temperature skyrmions in W/CoFeB/MgO thin films and microwires. *Applied Physics Letters*. 2017;111(2):022409. DOI:10.1063/1.4991360

38. Yang H, Thiaville A, Rohart S, Fert A, Chshiev M. Anatomy of Dzyaloshinskii-Moriya Interaction at Co/Pt Interfaces. *Physical Review Letters*. 2015;115(26):2672101(1-5). DOI:10.1103/PhysRevLett.115.267210

39. Han DS, Kim NH, Kim JS, Yin Y, Koo JW, Cho J, et al. Asymmetric hysteresis for probing Dzyaloshinskii-Moriya interaction. *Nano Letters*. 2016;16(7):4438-4446. DOI:10.1021/acs.nanolett.6b01593

40. Cho J, Kim NH, Lee S, Kim JS, Lavrijsen R, Solignac A, et al. Thickness dependence of the interfacial Dzyaloshinskii-Moriya interaction in inversion symmetry broken systems. *Nature Communications*. 2015;6:7635(1-7). DOI:10.1038/ncomms8635

41. Shahbazi K, Kim J Von, Nembach HT, Shaw JM, Bischof A, Rossell MD, et al. Domain-wall motion and interfacial Dzyaloshinskii-Moriya interactions in Pt/Co/Ir(tIr)/Ta multilayers. *Physical Review B*. 2019;99(9):094409(1-13). DOI:10.1103/PhysRevB.99.094409

42. Cui B, Li D, Yun J, Zuo Y, Guo X, Wu K, et al. Magnetization switching through domain wall motion in Pt/Co/Cr racetracks with the assistance of the accompanying Joule heating effect. *Physical Chemistry Chemical Physics*. 2018;20(15):9904-1-9. DOI:10.1039/c7cp08352a

43. Parkin S, Yang SH. Memory on the racetrack. *Nature Nanotechnology*. 2015;10(3):195-8. DOI:10.1038/nnano.2015.41

44. Ummelen F, Swagten H, Koopmans B. Racetrack memory based on in-plane-field controlled domain-wall pinning. *Scientific Reports*. 2017;7(1):1-8. DOI:10.1038/s41598-017-00837-x

45. Luo Y, Moske M, Samwer K. Interlayer coupling and magnetoresistance in Ir/Co multilayers. *Europhysics Letters*. 1998;42(5):565–570. DOI:10.1209/epl/i1998-00288-6

46. Pirro P, Hamadeh A, Lavanant-Jambert M, Meyer T, Tao B, Rosario E, et al. Perpendicularly magnetized CoFeB multilayers with tunable interlayer exchange for synthetic ferrimagnets. *Journal of Magnetism and Magnetic Materials*. 2017;432:260-265. DOI:10.1016/j.jmmm.2017.02.002

47. Chang YJ, Canizo-Cabrera A, Garcia-Vazquez V, Chang YH, Wu TH. Perpendicular magnetic tunnel junctions with synthetic antiferromagnetic pinned layers based on [Co/Pd] multilayers. *Journal of Applied Physics*. 2013;113(17):17B909(1-4). DOI:10.1063/1.4799974

48. Liu Y, Yu J, Zhong H. Strong antiferromagnetic interlayer exchange coupling in $[Co/Pt]_6/Ru/[Co/Pt]_4$ structures with perpendicular magnetic anisotropy. *Journal of Magnetism and Magnetic Materials*. 2019;473:381-386. DOI:10.1016/j.jmmm.2018.10.090

49. Nakajima N, Koide T, Shidara T, Miyauchi H, Fukutani H, Fujimori A, et al. Perpendicular magnetic anisotropy caused by interfacial hybridization via enhanced orbital moment in Co/Pt multilayers: magnetic circular X-ray dichroism study. *Physical Review Letters*. 1998;81(23):5229(1-4). DOI:10.1103/PhysRevLett.81.5229

50. Morgunov R, Hamadeh A, Fachec T, Lvovaa G, Koplak O, Talantsev A, Mangin S. Magnetic field and temperature control over Pt/Co/Ir/Co/Pt multistate magnetic logic device. *Superlattices and Microstructures*. 2017;104:509-517. DOI:10.1016/j.spmi.2017.02.033

51. Koplak O, Talantsev A, Lu Y, Hamadeh A, Pirro P, Hauet T, Morgunov R Mangin S. Magnetization switching diagram of a perpendicular synthetic ferrimagnet CoFeB/Ta/CoFeB bilayer. *Journal of Magnetism and Magnetic Materials*. 2017;433:91-97. DOI:10.1016/j.jmmm.2017.02.047

Информация об авторах / Information about the authors

Таланцев Артем Дмитриевич, кандидат физико-математических наук, младший научный сотрудник, ФГБУН «Институт проблем химической физики РАН», Черноголовка, Московская обл., Российская Федерация; ORCID 0000-0002-2223-4145; e-mail: artgtx32@mail.ru

Куницына Екатерина Игоревна, кандидат физико-математических наук, научный сотрудник, ФГБУН «Институт проблем химической физики РАН», Черноголовка, Московская обл., Российская Федерация; ORCID 0000-0002-8621-0740; e-mail: kunya_kat@mail.ru

Моргунов Роман Борисович, доктор физико-математических наук, профессор, главный научный сотрудник, ФГБУН «Институт проблем химической физики РАН», Черноголовка, Московская обл.; ФГБОУ ВО «Тамбовский государственный технический университет», Тамбов, Российская Федерация; ORCID 0000-0002-4859-2733; e-mail: morgunov2005@yandex.ru

Artem D. Talantsev, Cand. Sc. (Physics and Mathematics), Junior Researcher, Institute of Problems of Chemical Physics of Russian Academy of Sciences, Chernogolovka, Moscow region, Russian Federation; ORCID 0000-0002-2223-4145; e-mail: artgtx32@mail.ru

Ekaterina I. Kunitsyna, Cand. Sc. (Physics and Mathematics), Researcher, Institute of Problems of Chemical Physics of Russian Academy of Sciences, Chernogolovka, Moscow region, Russian Federation; ORCID 0000-0002-8621-0740; e-mail: kunya_kat@mail.ru

Roman B. Morgunov, D. Sc. (Physics and Mathematics), Professor, Chief Researcher, Institute of Problems of Chemical Physics of Russian Academy of Sciences, Chernogolovka, Moscow region; Tambov State Technical University, Tambov, Russian Federation; ORCID 0000-0002-4859-2733; e-mail: morgunov2005@yandex.ru

Received 25 June 2021; Accepted 09 August 2021; Published 30 September 2021

Copyright: © Talantsev AD, Kunitsyna EI, Morgunov RB, 2021. This article is an open access article distributed under the terms and conditions of the Creative Commons Attribution (CC BY) license (https://creativecommons.org/licenses/by/4.0/).